Data Repository Item 2002103

Supplementary Material for "Sedimentologic-Magnetic Record of Western Pangean Climate in Upper Paleozoic Loessite (Lower Cutler Beds, Utah)

G.S. (Lynn) Soreghan, R. Douglas Elmore, and Michael T. Lewchuk

(for GSA Data Repository)

Paleomagnetic and Rock magnetic Methods

Most of the cores were oriented with an inclinometer and Brunton compass. All cores (715) were cut to standard length, and weight-normalized bulk magnetic susceptibility (χ_b) was measured on a Sapphire SI-2 Instrument. The natural remanent magnetizations (NRMs) were measured on a 2G three-axes cryogenic magnetometer located in a magnetically shielded room. A representative set of specimens was selected for stepwise demagnetization by alternating field (AF) demagnetization (n = 33) up to 100 mT in a 2G Automated Degaussing System and by thermal demagnetization (n = 49) up to 700°C in an Schonstedt TSD-1 oven. The decay patterns were displayed in orthogonal projections (Zijderveld, 1967) and line segments were identified. Principal component analysis (Kirschvink, 1980) was performed to identify the components. The mean angular deviation (MAD) angles were less than 15°.

An impulse magnetizer was used to obtain the acquisition pattern of an isothermal remanent magnetization (IRM). This was followed by thermal decay of three perpendicular IRMs (Lowrie, 1990) with fields of 120 mT, 500 mT and 2500 mT.

The thermal decay patterns of low-temperature SIRMs were recorded on a Magnetic Property Measurement System (MPMS) at the Institute for Rock Magnetism, University of Minnesota, for samples from several representative loessite/paleosol couplets. These data were used to estimate the amount of SP grains, which is the difference in remanence between 50K and 300K, after subtracting the drop in remanence at the Verwey transition. The decrease between 50-300 K should be used to infer a SP contribution because low-temperature ordering in clays and other minerals, and temperature-dependent magnetocrystalline anisotropy and/or magnetostriction can conribute to the decrease below 50K (M. Jackson, personal communication).

Paleomagnetism and Rock Magnetism of the Lower Cutler Beds

Alternating field demagnetization from 30 to 100 mT removed a linear component of magnetization in about half of the specimens analyzed (Figs. 1a, 2). The mean direction for this component is declination 10.5°, inclination 57.9° (n/n_o = 16/33, α_{95} = 10.2°, k = 14.0) and the pole position is 81.6°N, and 33.3°W. The cone of confidence includes both the Present Earth's Field, the modern dipole field, as well as part of the Tertiary apparent polar wander path (APWP). The AF treatment removes a significant fraction of the magnetization (mean = 34.5%, standard deviation = 22.0%, n=31) with a range from 6% to 98%. The amount of AF decay in paleosols (36%, standard deviation = 11%) was higher than that in loessite (29%, standard deviation = 14%) although the standard deviations overlap.

Thermal demagnetization at low temperatures (NRM to 300°C) of most specimens removes a northerly and steeply down magnetization that is interpreted to be a Cenozoic viscous remanent magnetization (VRM). At higher temperatures a characteristic remanent magnetization (ChRM) with southeasterly declinations and shallow inclinations is removed in about half (26/60) of the specimens (Fig. 1b, Fig. 2). The decay in these specimens ranges from a gradual, thermally-distributed unblocking temperature pattern (Fig. 1b) to a more thermally discrete pattern with most of the decay at temperatures above 640°C. The mean direction for the ChRM is D=150.7°, I=-4.3° (N/N_o=26/60, k=21, α_{95}=6.0°) in geographic coordinates moves slightly to D=152.4°, I=-7.8 in stratigraphic coordinates (k=18, α_{95}=6.5°) with a negligible change in the statistical parameters.

The magnetization in most of the other specimens exhibits erratic decay and linear components could not be isolated. In a few specimens from one interval a magnetization with northwesterly declinations and shallow inclinations was removed. The NRM intensities are up to 100 times as strong as the other samples, the decay is linear without a VRM, and the magnetization is removed by AF treatment.

The samples are from one limb of an anticline with a slight variation in dip so the fold test was not applicable. However, both the geographic and stratigraphic directions yield Paleozoic directions and the deformation is Laramide (Krantz, 1989) so the magnetization must have been acquired prior to tilting. The stratigraphic direction yields a pole at 114.6° E, 48.4° N (A_{95}=4.6°, Khramov, 1987) which falls near the middle to late Permian part of the apparent polar wander path (Fig. 3), significantly younger than the age of the strata. However, given a 7.3° clockwise rotation of the Colorado Plateau (Molina Garza et al., 1998), and a vertical axis rotation about the site location, the mean direction moves to D=145.1°, I=-7.8°, shifting the pole to a position (123.0° E, 44.0° N) coincident with the early Permian reference pole of 123° E, 45° N (267-281 Ma; Van der Voo, 1993).

Acquisition curves of IRMs for samples from the Cutler Formation show a rapid rise by 100 mT and then a more gradual rise up to 2500 mT (Fig. 4a). This suggests that a low coercivity phase is present but that the remanence is dominated by a high coercivity phase. Subsequent stepwise thermal demagnetization of a tri-axial IRM (Lowrie, 1990) reveals that the low coercivity component decays by 580^{o}C which indicates the presence of magnetite (Fig. 4b). The intermediate and high coercivity components decay gradually up to about 640-660^{o}C where the remaining IRM (~ 15 %) generally decays abruptly (Figure 4b). This confirms the presence of hematite. Curie balance analyses of several samples did not reveal any magnetic minerals other than hematite (Cogoini et al., 2001). These results indicate the remanence is dominated by hematite, although some magnetite is present.

Patterns of thermal demagnetization of low-temperature SIRMs were recorded for the profiles to investigate the contribution of supermparamagnetic (SP) magnetite to the χ_b signal (Figs. 5-7). The results of these analyses for samples from three of the profiles show a steeper initial drop in remanence for the paleosols relative to the more loessitic samples (Figs. 5 and 6; Fig. 7 in manuscript) with higher amounts of SP material in the paleosol compared to the loessite. In one paleosol (Fig. 7), a protosol, there are no vertical trends in the amount of SP material. The remanence at room termperature, however, also increases up-profile in all paleosols (Figs. 5-7; Fig. 7 in manuscript).

Some of the low-temperature curves also show an attenuated Verwey transition at around 110^{o}K which is indicative of mostly multidomain (md) magnetite (Cogoini et al., 2001). The Verwey, however, is poorly devloped which could be indicative of oxidation and maghemitization of magnetite (Özdemir et al., 1993).

REFERENCES

Cogoini, M., Elmore, R.D., Soreghan, G.S., and Lewchuk, M., 2001, Contrasting rock-magnetic characterisitics of two upper Paleozoic loessite-paleosol profiles: Physics and Chemistry of the Earth, v. 26, p.905-910.

Fisher. R. A., 1953, Dispersion on a sphere: Proceedings of the Royal Society of London, v. A217, 295-305.

Kirschvink, J.L., 1990 The least-squares line and plane and the analysis of paleomagnetic data, Geophysical Journal of the Royal Astronomical Society, v. 62, p. 699-718.

Krantz, R.W., 1989, Laramide structures of Arizona, *in* Jenney, J.P., and Reynolds, S.J., eds., Geologic Evolution of Arizona: Arizona Geological Society Digest, v. 17, p. 463-483.

Khramov, A.K. 1987. Paleomagnetology, Springer-Verlag, Berlin, 308 p.

Lowrie, W., 1990, Identification of ferromagnetic minerals in a rock by coercivity and unblocking temperature properties: Geophysical Research Letters, v. 17, p. 159-162.

Molina Garza, R.S., Acton, G.D., and Geissman, J.W., 1998, Carboniferous through Jurassic paleomagnetic data and their bearing on rotation of the Colorado Plateau: Journal of Geophysical Research, v. 103, p. 24,179-24,188.

Özdemir, O., Dunlop, D.J., and Moskowitz, B.M., 1993, The effect of oxidation on the Verwey transition in magnetite: Geophysical Research Letters, v. 20, p. 1671-1674.

Van der Voo, R., 1993, Paleomagnetism of the Atlantic, Tethys and Iapetus Oceans, Cambridge University Press, Cambridge, 411 p.

Zijderveld, J.D.A., 1967 A.c. demagnetization of rocks: Analysis of results, *in* Collinson, D.W., Creer, K.M., and Runcorn S.K (eds.), Methods in Paleomagnetism: Elsevier, p. 254-286.

FIGURE CAPTIONS

Figure 1.

Orthogonal projections of the typical thermal demagnetization behavior (temperature steps in ^{o}C). a) Alternating field demagnetization removes a northerly and down component in some specimens at coercivities between 20 and 70 mt. b)Specimen showing removal of a northerly and down component at low temperatures, interpreted as a modern VRM, and gradual removal of a component with southeasterly declinations and equatorial inclinations at higher temperatures. Squares represent the vertical component, circles represent the horizontal component.

Figure 2.

Equal area stereonet plot showing specimen directions from the lower Cutler beds in stratigraphic coordinates. Solid symbols are lower hemisphere projections, open symbols are upper hemisphere projections. Squares are component removed by AF demagnetization whereas circles are components removed by thermal treatment.

Figure 3.

Apparent Polar Wander Path with reference poles and the 95% confidence width (Van der Voo, 1993) showing the overall mean direction in stratigraphic coordinates, circumscribed by the cone of 95% confidence. The arrow indicates the sense of change in the pole position given a 7.3° clockwise rotation of the Colorado Plateau.

Figure 4.

Representative IRM acquisition (a) and thermal triaxial decay (b) curves for a lower Cutler bed sample. The steep slope below 100 mT in the acquisition curve suggests a low coercivity phase is present and the rise above 200 mT indicates the presence of a high coercivity phase. The decay of the low coercivity component by 580^{o}C indicates that the low coercivity phase is magnetite. Decay of the high coercivity component to 680^{o}C indicates that hematite is present.

Figure 5.

Thermal demagnetization of low-temperature SIRMs and cooling curves from an Argillisol at 118.2-119.4 (see Fig. 6c in manuscript). 5a) 118.75, b) 119.1, c) 119.3, d) 119.4.

Figure 6.

Thermal demagnetization of low-temperature SIRMs and cooling curves from an Argillisol 137.8-138.7 (see Fig. 6d in manuscript). 6a) 137.8, b) 138.35, c) 138.6.

Figure 7.

Thermal demagnetization of low-temperature SIRMs and cooling curves from a Protosol 119-120 (see Fig. 6b in manuscript). 7a) 120.0, 7b) 120.3, c) 120.35.

(a)

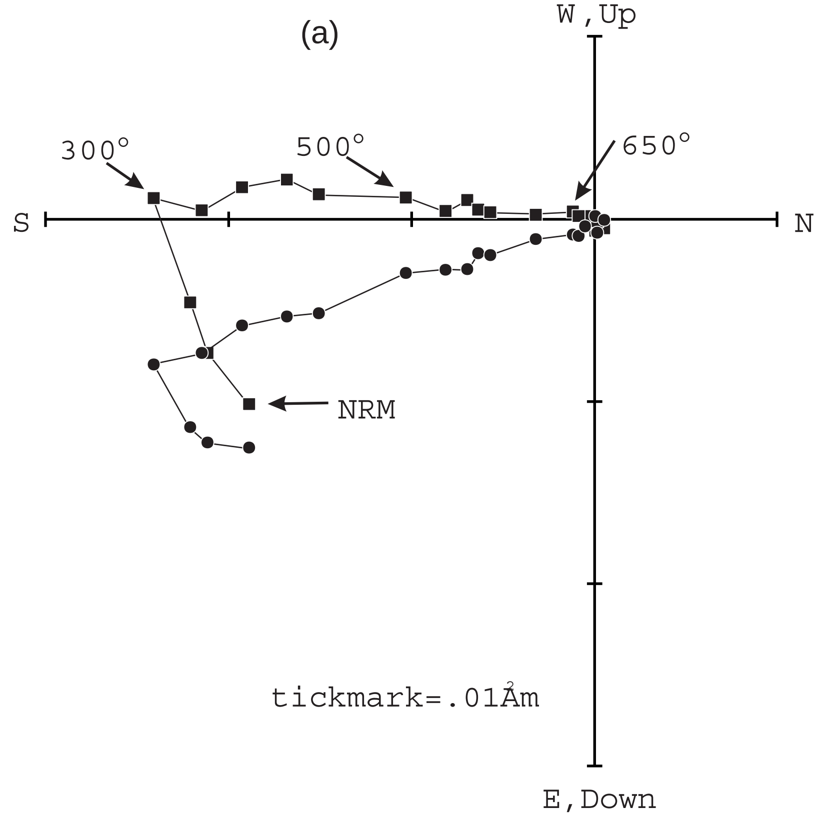
W,Up
300°
500°
650°
S
N
NRM
tickmark=.01Åm²
E,Down

(b)

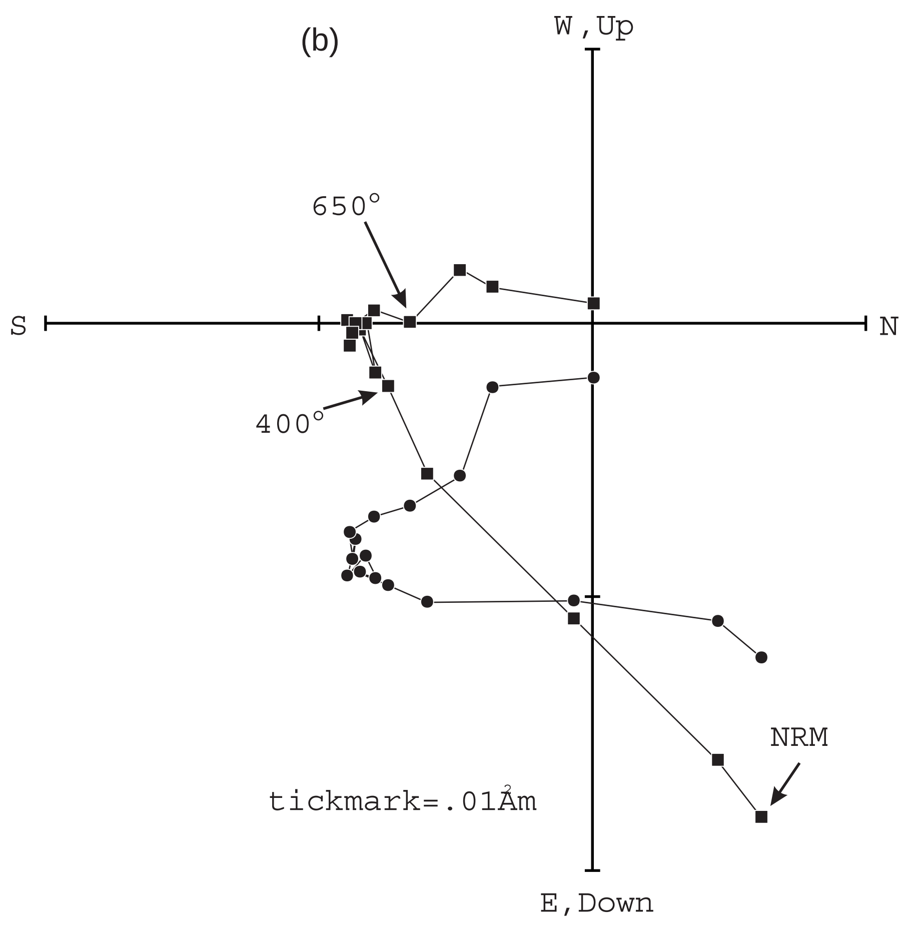
W,Up
650°
S
N
400°
NRM
tickmark=.01Åm²
E,Down

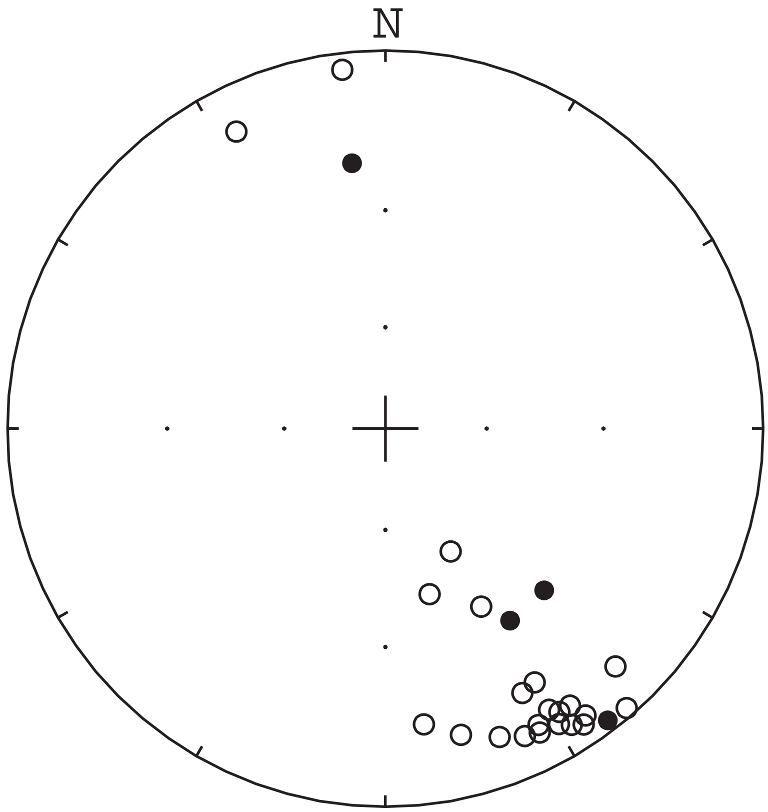
N

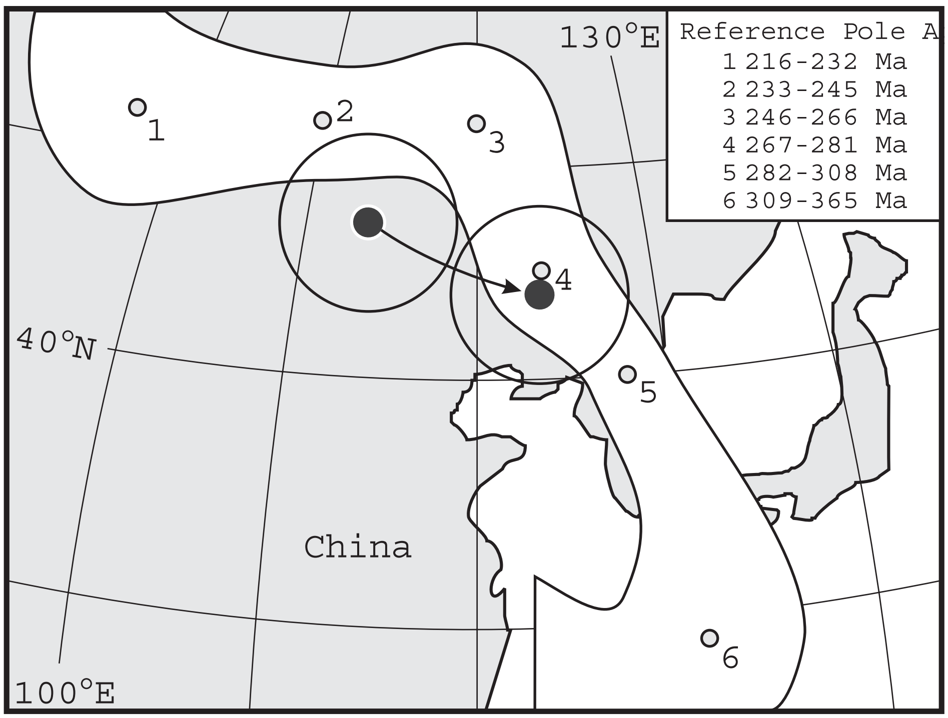

Reference Pole A
1 216-232 Ma
2 233-245 Ma
3 246-266 Ma
4 267-281 Ma
5 282-308 Ma
6 309-365 Ma
130°E
40°N
100°E
China
1
2
3
4
5
6

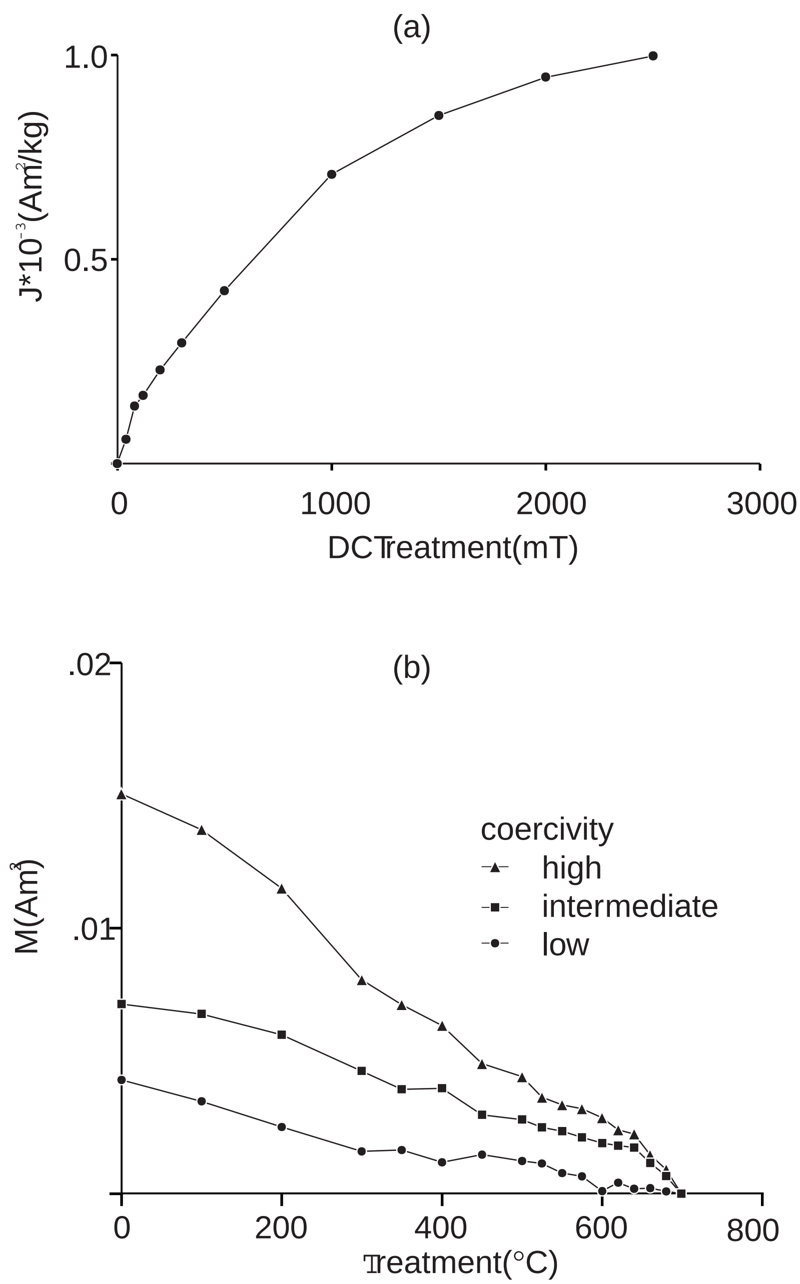
(a)
1.0
0.5
J*10⁻³(Am²/kg)
0
1000
2000
3000
DC Treatment(mT)
(b)
.02
.01
M(Am²)
coercivity
high
intermediate
low
0
200
400
600
800
Treatment(°C)

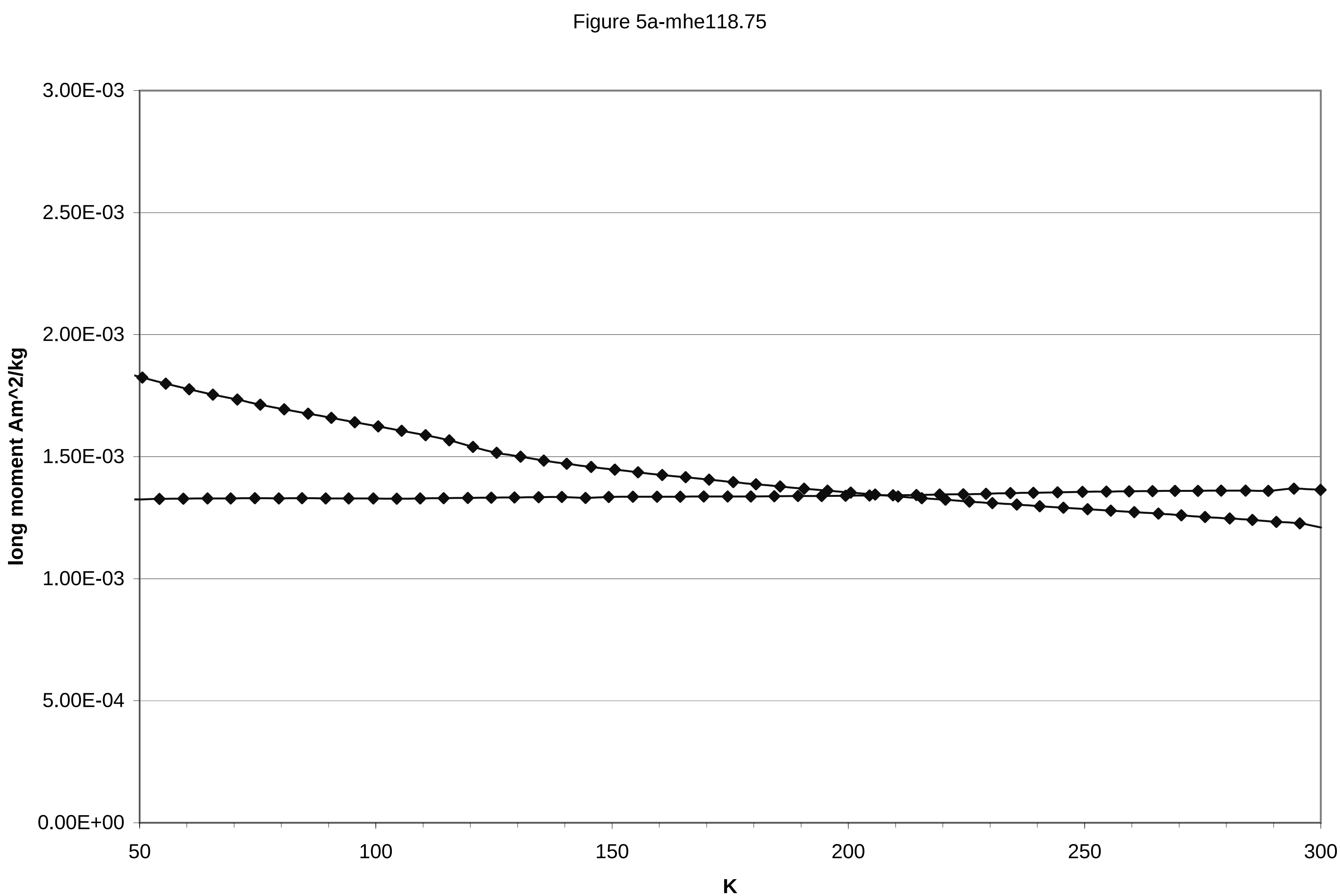

Figure 5a-mhe118.75
3.00E-03
2.50E-03
2.00E-03
1.50E-03
1.00E-03
5.00E-04
0.00E+00
long moment Am^2/kg
50
100
150
200
250
300
K

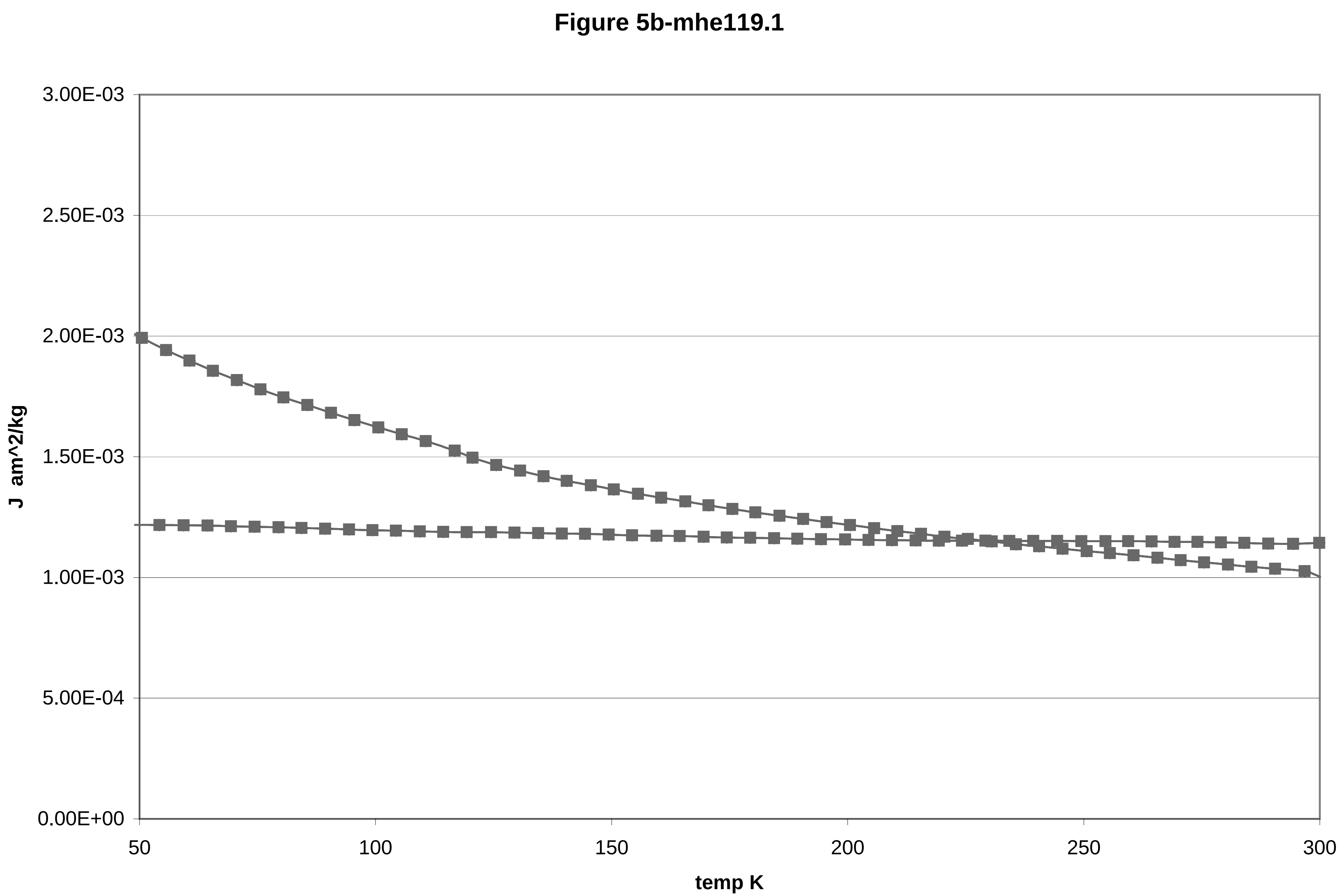
Figure 5b-mhe119.1
3.00E-03
2.50E-03
2.00E-03
1.50E-03
1.00E-03
5.00E-04
0.00E+00
J am^2/kg
50
100
150
200
250
300
temp K

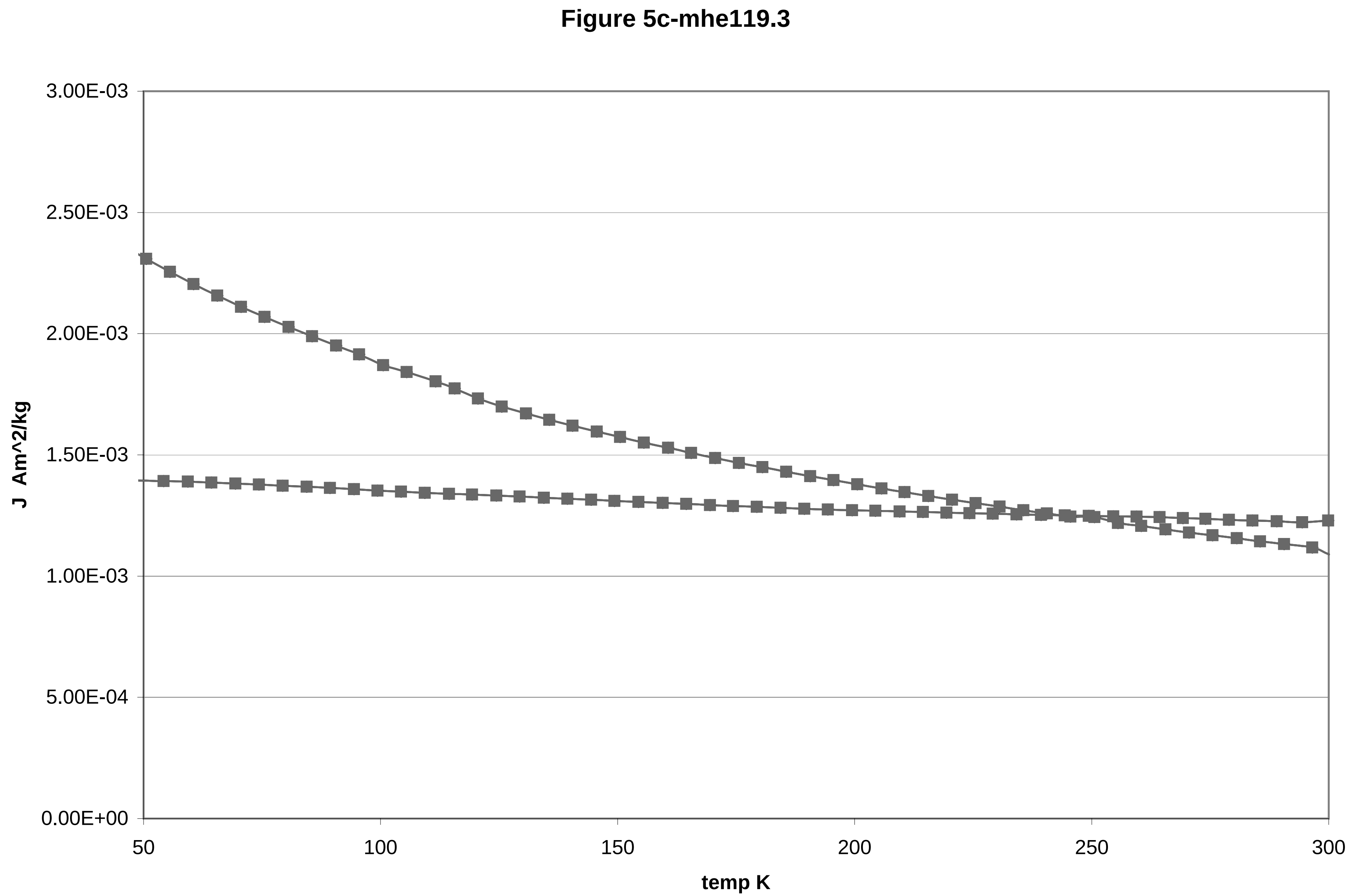
Figure 5c-mhe119.3
3.00E-03
2.50E-03
2.00E-03
1.50E-03
1.00E-03
5.00E-04
0.00E+00
J Am^2/kg
50
100
150
200
250
300
temp K

Figure 5d-mhe119.4

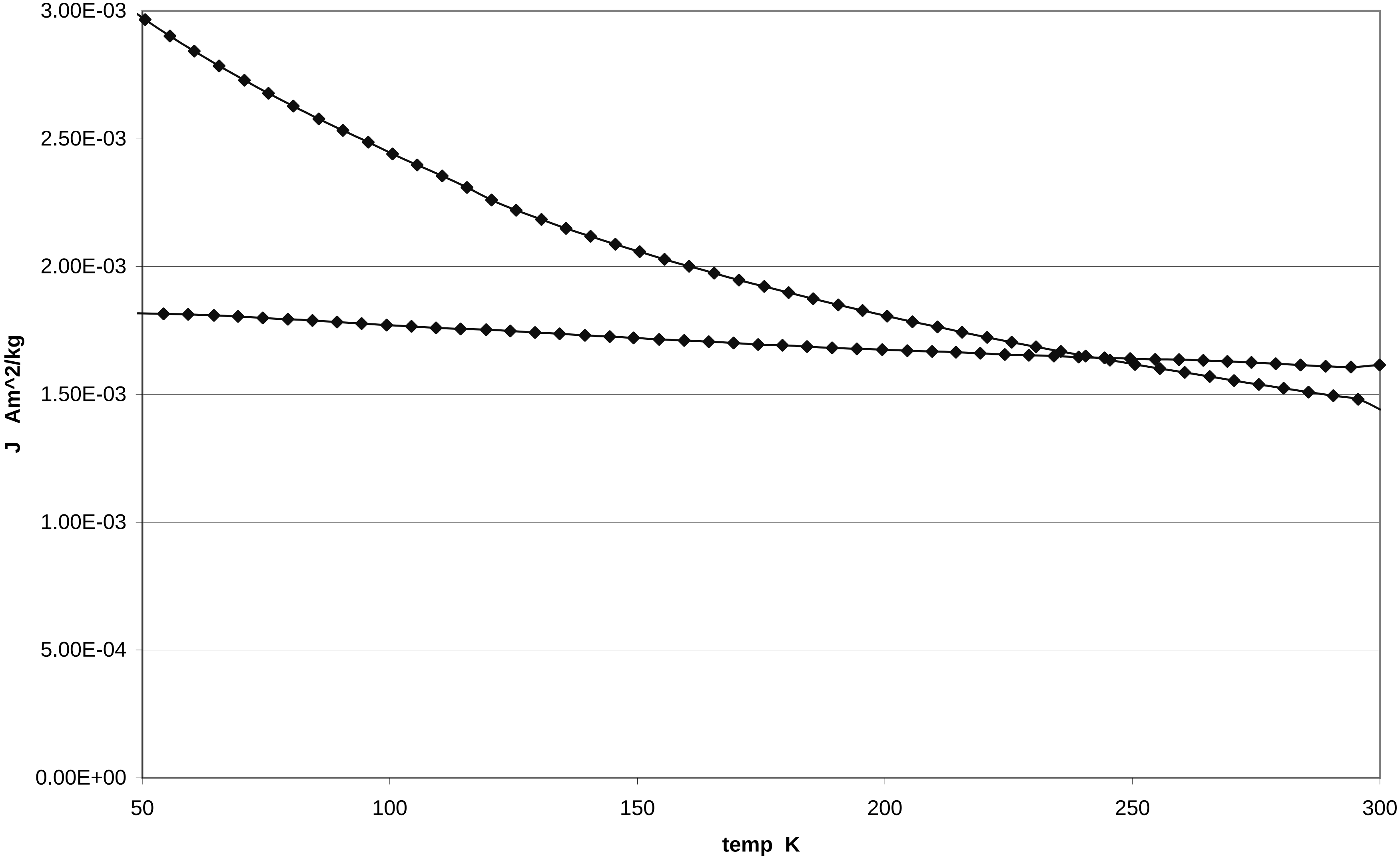

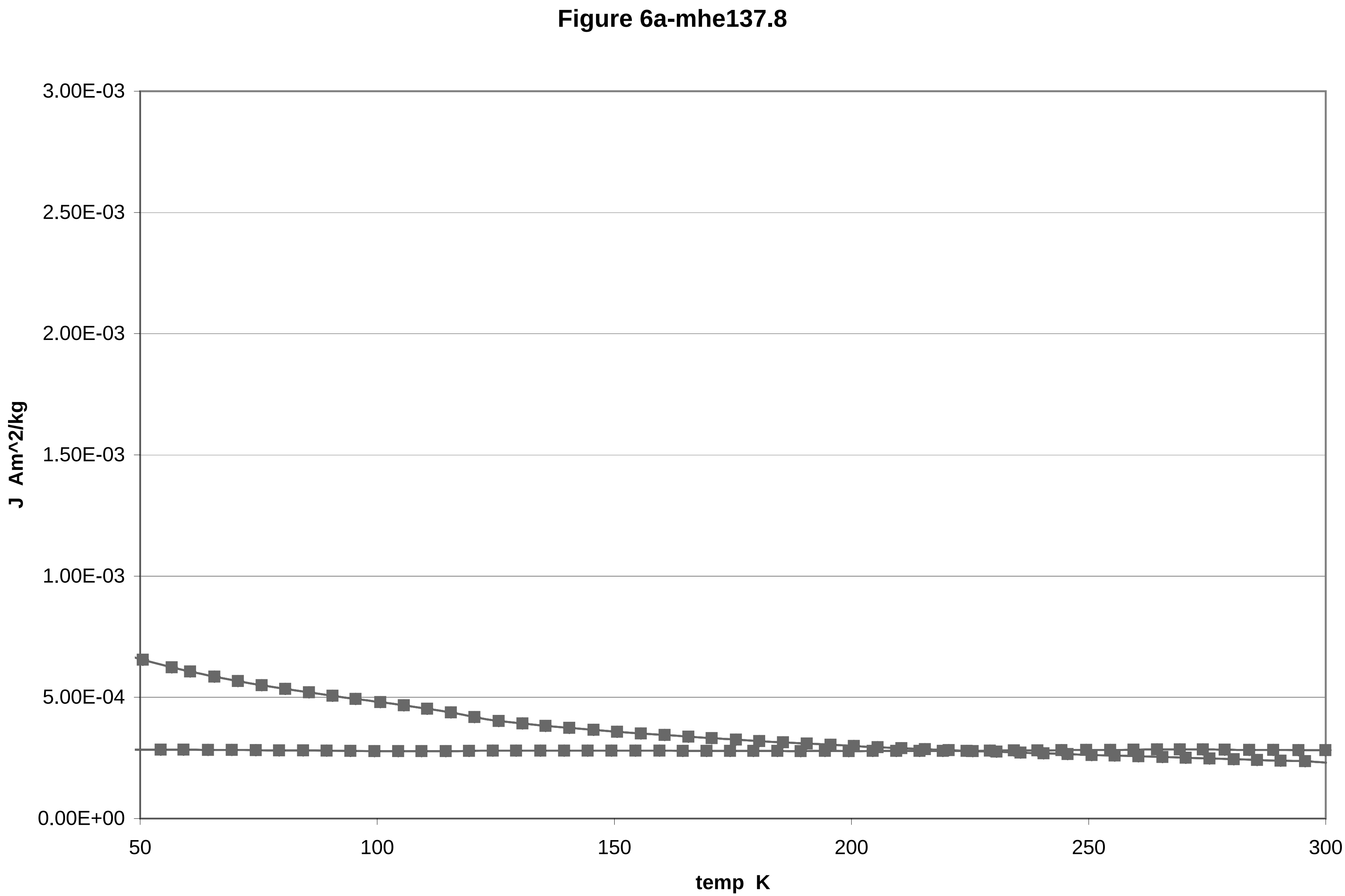

Figure 6a-mhe137.8
3.00E-03
2.50E-03
2.00E-03
1.50E-03
1.00E-03
5.00E-04
0.00E+00
J Am^2/kg
50
100
150
200
250
300
temp K

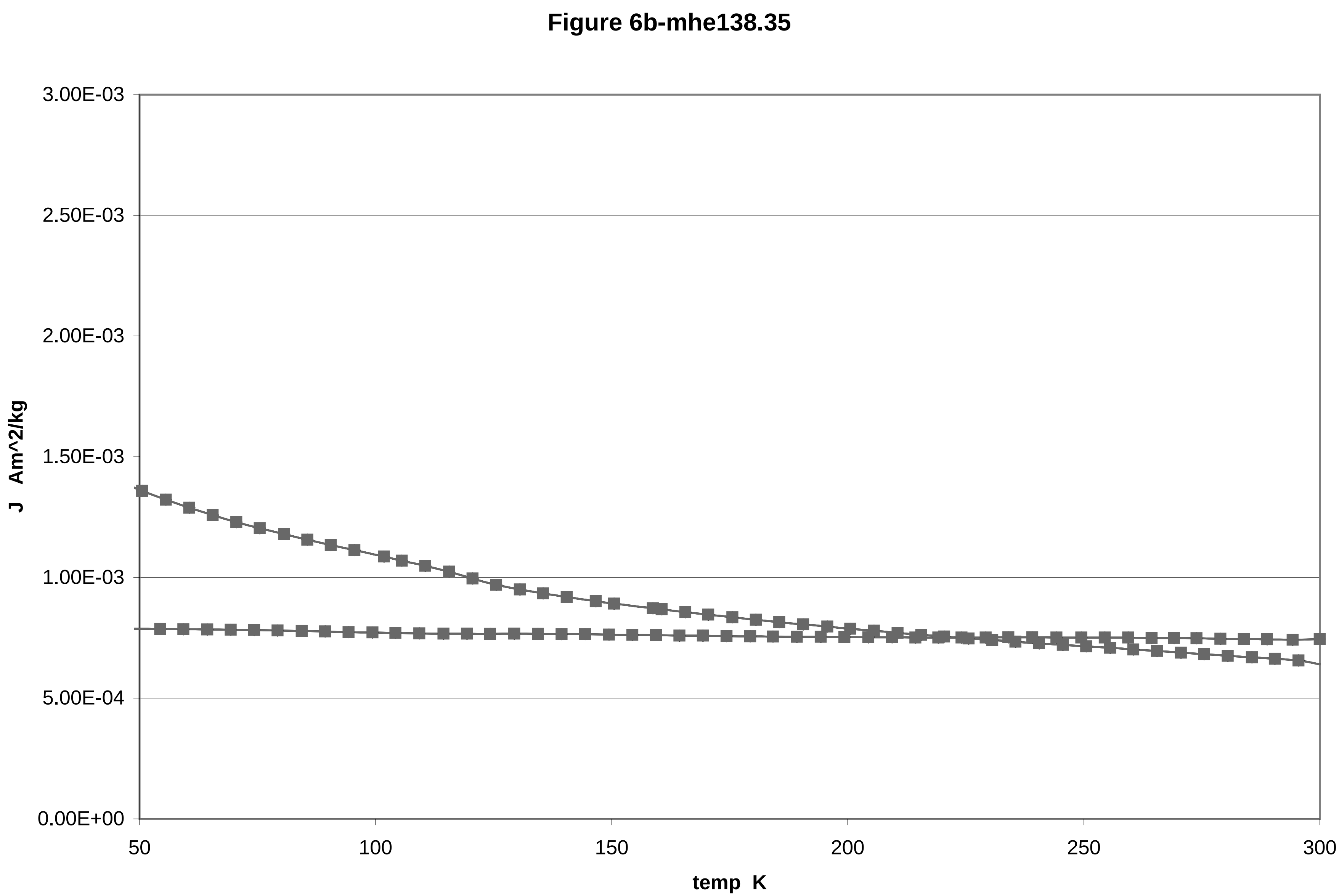
Figure 6b-mhe138.35
3.00E-03
2.50E-03
2.00E-03
1.50E-03
1.00E-03
5.00E-04
0.00E+00
J Am^2/kg
50
100
150
200
250
300
temp K

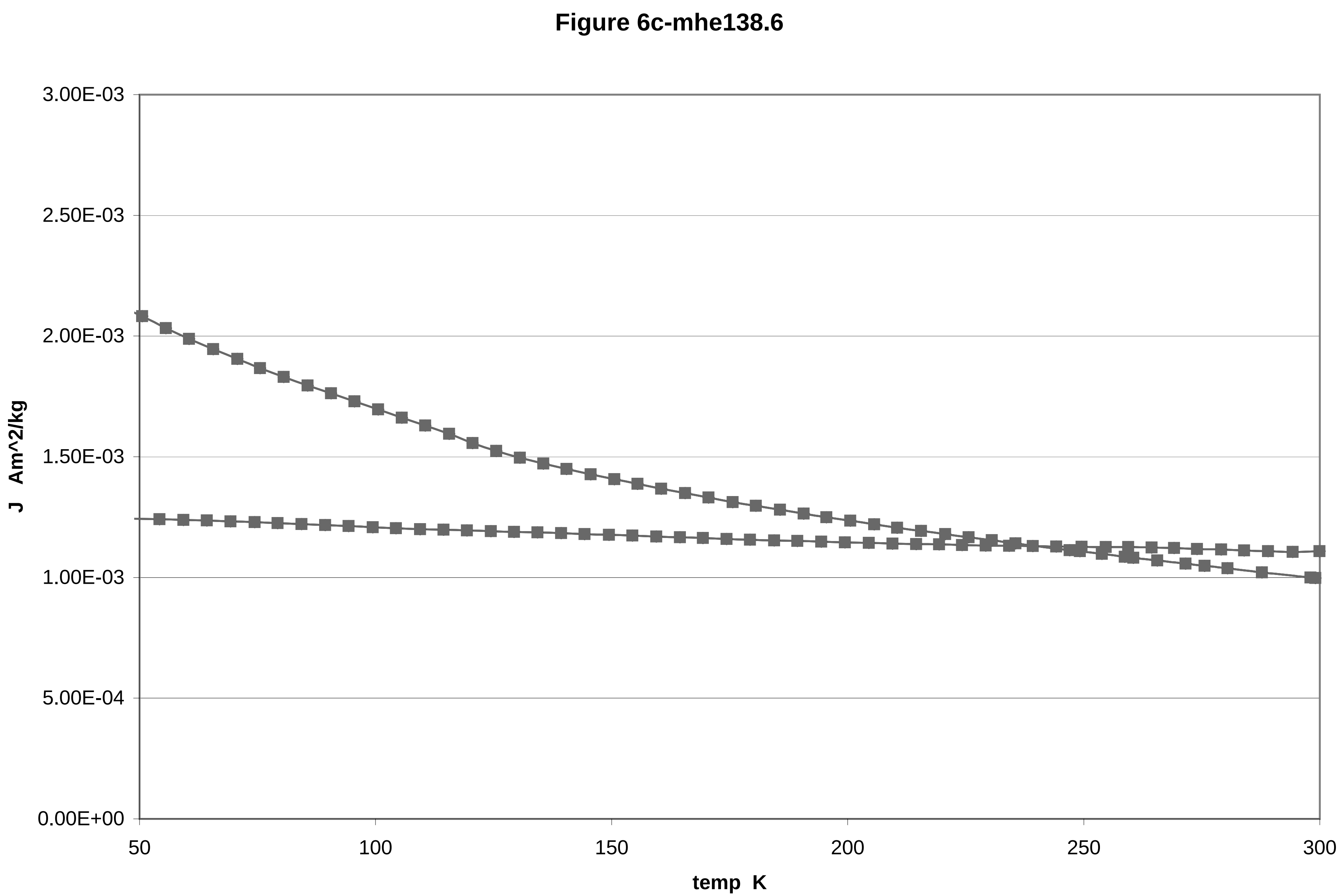
Figure 6c-mhe138.6
3.00E-03
2.50E-03
2.00E-03
1.50E-03
1.00E-03
5.00E-04
0.00E+00
J Am^2/kg
50
100
150
200
250
300
temp K

Figure 7a-mhe120.0

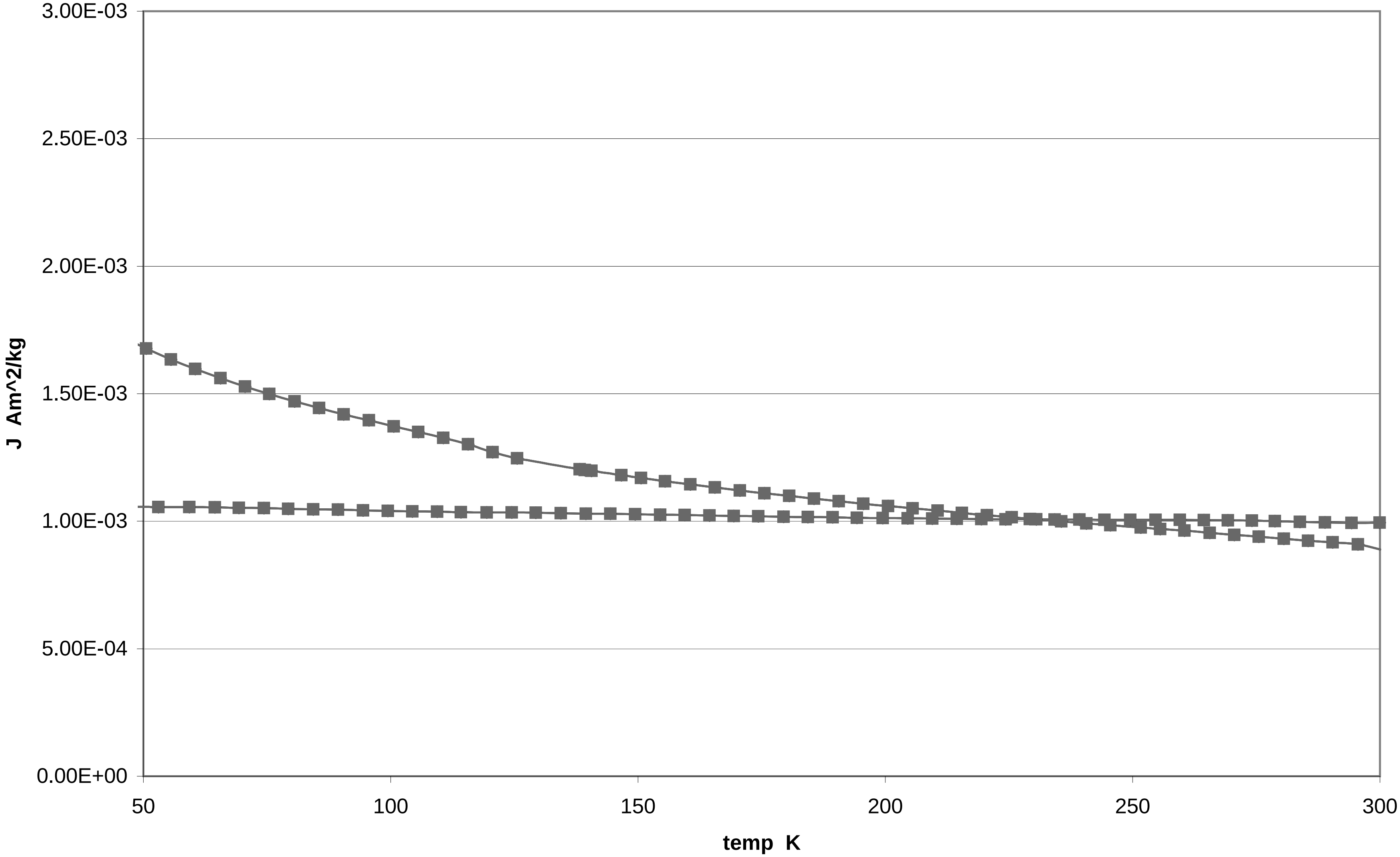

Figure 7b-mhe120.3

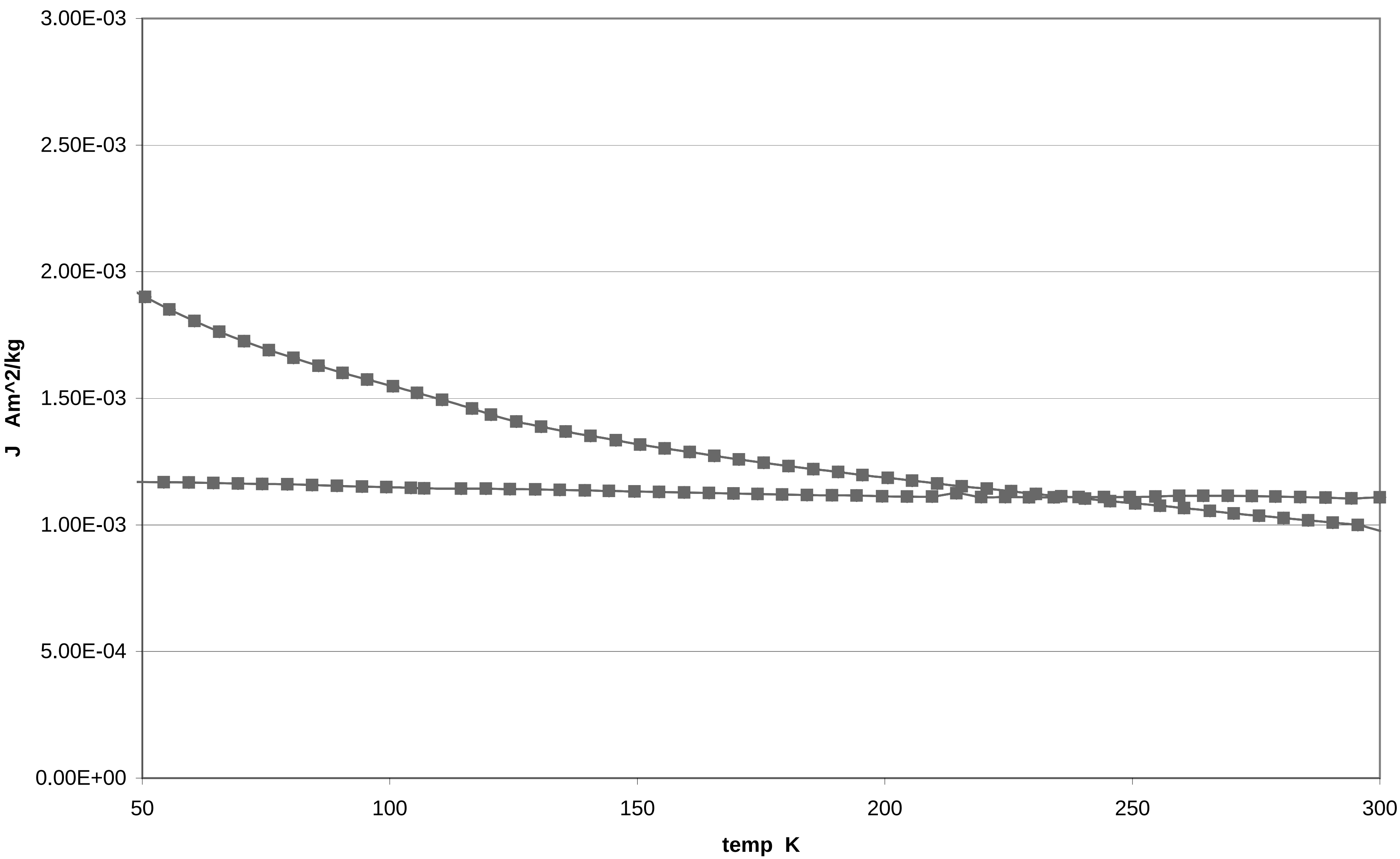

Figure 7c-mhe120.35